MicroBooNE–Note–1032–PUB v1.3

First Measurement of Muon Neutrino Charged Current Single Neutral Pion Production on Argon with the MicroBooNE LArTPC

(MicroBooNE Collaboration)

(Dated: 31 May 2018)

We report the first measurement of the absolute flux-integrated cross section of ν_μ *charged current single* π^0 *production on argon. This measurement was performed with the MicroBooNE detector, a liquid argon time projection chamber, utilizing neutrinos produced by the Fermilab Booster Neutrino Beam. The analysis uses the first fully automated electromagnetic shower reconstruction employed to analyze data from a liquid argon time projection chamber.*

I. Introduction

Neutrino experiments have begun employing liquid argon time projection chambers (LArTPC) [1] due to their fully active readout volume, homogeneous nuclear target, and millimeter-scale spatial resolution. In addition, the calorimeteric information of the particles that pass through the argon coupled with the spatial resolution enables the efficient separation of electromagnetic (EM) showers produced by electrons and photons [2]. This capability has made it the detector of choice for future electron-neutrino appearance experiments such as DUNE [3] and the SBN Program [4]. MicroBooNE [5] is the first large-scale surface LArTPC to be deployed in a neutrino beam. The primary physics goal of MicroBooNE is to test MiniBooNE results which showed an anomalous excess of electron-neutrino-like events between $200 - 600$ MeV in reconstructed neutrino energy [6]. To achieve the varied physics goals of these LArTPC experiments, an efficient and fully automated reconstruction of the events is necessary. This note reports the first application of a fully automated shower reconstruction. This novel reconstruction is then used to perform the first measurement of ν_μ charged current single π^0 production on argon. This process is characterized by the presence of a μ in conjunction with a π^0 that decays promptly into two photons accompanied by any number of additional non-π^0 hadrons.

Neutral pions present a potential background to electron neutrino appearance searches, as photons can mimic electrons in detectors. This problem is especially acute in the case that one photon from the decay is not detected, or the two photon showers are merged. Accurate modeling of pion production processes becomes important at DUNE energies, where the resonant channel contributions are large. In addition, final state interactions (FSI) of pions as they travel through the nucleus depend on the nuclear environment, which is presently poorly understood. Measurements in argon will lead to better understanding of these processes.

Charged current neutral pion production has been studied in neutrino scattering off several nuclear targets, including with hydrogen and deuterium, performed by bubble chamber experiments at ANL [7] and BNL [8 and 9], Minerνa [10 and 11], SciBooNE [12], and MiniBooNE [13] in carbon. The Minerνa measurement is at higher neutrino energies than this result, but the SciBooNE and MiniBooNE experiments both operated in the Booster Neutrino Beam (BNB), where MicroBooNE is situated.

II. Experimental Setup

This measurement is performed using neutrinos originating from the BNB [14]. The beam creates a 93.6% pure source of ν_μ, with an average energy of 800 MeV. The neutrinos impinge upon the MicroBooNE detector at a distance of 470 m from the target station. The detector is an 85 tonnes fully active LArTPC [5] which is read out at the anode by three planes of sense wires situated 256 cm from a cathode, held at −70 kV. Ionization electrons cross the full drift distance in 2.3 ms. The first two sense planes record induced signals while the final sense plane collects the charge. In this result we use only the final (collection) plane to provide calorimetric information about the particles traversing the detector. The scintillation light produced is collected by an array of 32 photo-multiplier tubes (PMTs). Light collected by the PMTs in-time with the 1.6 μs beam-spill is used to trigger a 4.8 ms TPC readout window.

III. Simulation

We simulate the flux of neutrinos at MicroBooNE using the framework built by the MiniBooNE collaboration along with their uncertainties. To simulate these neutrinos interacting with nuclei in our detector, along with the relevant nuclear processes that modify the final-state, we employ the GENIE event generator [15]. Beyond the default configuration we also enable a empirical handling of meson exchange current (MEC) interactions which populate multi-nucleon final states [16]. The particles that exit these interactions are then passed to a custom implementation of GEANT4 available in the LArSoft software toolkit [17]. Cosmic background events that produces activity that coincides with the beam-spill and triggers a readout is measured directly in data by utilizing a pulsed trigger that collects data non-coincident with the beam exposure. Cosmic backgrounds that do not produce activity that coincides with the beam spill and triggers a readout is modeled with CORSIKA at an elevation of 226 m above sea level [18].

IV. Reconstruction and Event Selection

We reconstruct the neutrino interactions with algorithms available in LArSoft. This begins by taking the raw signals on our three sense wire planes, filtering electronics noise [19], and processing our signals to isolate Gaussian shaped signals [20 and 21], known as *hits*. From these hits the Pandora event reconstruction toolkit [22] is used to cluster the hits and create 3D track and vertex objects that can be associated back to particles in our detector. These 3D vertices are candidate locations for neutrino interactions and we aim to identify the correct one in the next section to act as a seed for our shower reconstruction stage.

To remove cosmic particles tracks we reject tracks that are clearly through-going. We also remove, as a cosmic background, any track that is inconsistent with the spatial distribution of light on the PMT array used to open the trigger window. The tracks that remain after this initial cosmic rejection are passed to an inclusive ν_μ charged current preselection and treated as candidate μ. Being a surface detector with a relatively long readout window, cosmics form a major challenge in this analysis. In every readout window we expect to collect upwards of 20 cosmic particles. Sitting relatively far from the beam source also means that at triggering only 1 in 30 readout windows will contain a real neutrino interaction. This presents two challenges, the first is selecting true neutrino interactions and distinguishing muon tracks originating from ν_μ charged current interactions from cosmic muons. The second challenge is collecting the hits on a single plane which are associated to the same particle. For particles that are reconstructed as tracks this can be more straightforward than for EM showers. We begin to address this by trying to anchor our clustering at the start point of a candidate muon from an inclusive ν_μ charged current interaction.

A candidate ν_μ induced μ is selected if its deposited charge is consistent with the spatial distribution of light collected on the PMT array during the trigger and has a length, L, greater than 15 cm. We also require

- one of the candidate muon track end-points to be displaced less than 3 cm from a 3D reconstructed vertex,
- the vertex to be within a fiducial volume of 10 cm from the up- and down-stream faces of the detector (z), 20 cm from the anode and cathode planes (x), and 20 cm from the top and bottom of the TPC (y), and
- all other tracks with end-points within 3 cm of the vertex are considered to have come from the candidate neutrino interaction point.

These cuts provide us with a candidate ν_μ induced muon and a candidate vertex. We reject cosmic backgrounds by employing multiplicity-dependent cuts. For events that contain a single track associated to the vertex, we require

- the track to be fully contained with the predefined fiducial volume,
- the track to have the fraction of its momentum in the y-direction, $p_y/|p|$, be less than 0.4, and
- the track end higher in y to deposit more energy then the end lower in y if the track has a projected length in y, L_y, less than 25 cm.

These cuts help us to remove cosmic tracks that would be entering through the top of the TPC volume and coming to rest, with a Bragg peak. For vertices with more than a single track we require that

- the two longest tracks not be back-to-back, $\theta_{12} < 155°$, and

- the second longest track have length $L > 30$ cm or have $p_y/|p| < 0.65$ if the longest track ends at a higher y position than the other tracks.

These cuts help remove instances where a single cosmic particle is broken into two back-to-back tracks. Finally, for vertices with exactly two tracks we require

- the second longest track have $L > 30$ cm,
- either the end-point of the muon candidate must have an absolute y-position < 96.5 cm, or
- the tracks have energy deposition profiles inconsistent with a stopping muon decaying to an electron.

These requirements are carefully tuned to help mitigate cases where a cosmic muon comes to rest in the detector volume and decays to a Michel electron. To verify that our muon candidate is consistent with a minimally ionizing particle we require

- the mean hit charge within one RMS of the median hit charge for the candidate muon track be consistent with a minimally ionizing particle (to distinguish it from a proton) and
- no deflections of greater than 8° along the candidate muon track (to distinguish it from a misreconstructed EM shower).

With these requirements, we select events that have a muon candidate attached to a vertex and have greatly mitigated cosmic backgrounds. We use the vertex as an anchor point for the EM shower reconstruction, discussed later in this section.

Our data sample consists of 1.62×10^{20} protons on target, after passing data and beam quality requirements, collected between February 2016 and July 2016. The preselection reduces the number of readouts containing only cosmic activity by 99.9%, creating a sample of events that is 80% pure in ν_μ charged current interactions with a 33% signal efficiency. The fraction of selected ν_μ charged current interactions that produced a single π^0 is 6%. To identify these events we employ a novel second pass automated reconstruction for photon showers emanating from an interaction vertex.

The goal of this stage of reconstruction is distinguishing EM showers associated to the neutrino interaction from uncorrelated cosmic activity. To aid in this we separate the EM reconstruction into two stages: the first aims to identify hits that are due to neutrino induced EM showers and the second clusters these hits into individual showers. The first stage begins by seeding the EM shower reconstruction on each readout plane with the output of an early clustering pass performed by Pandora. The Pandora clustering pass is intended to gather charge from only a single particle without collecting

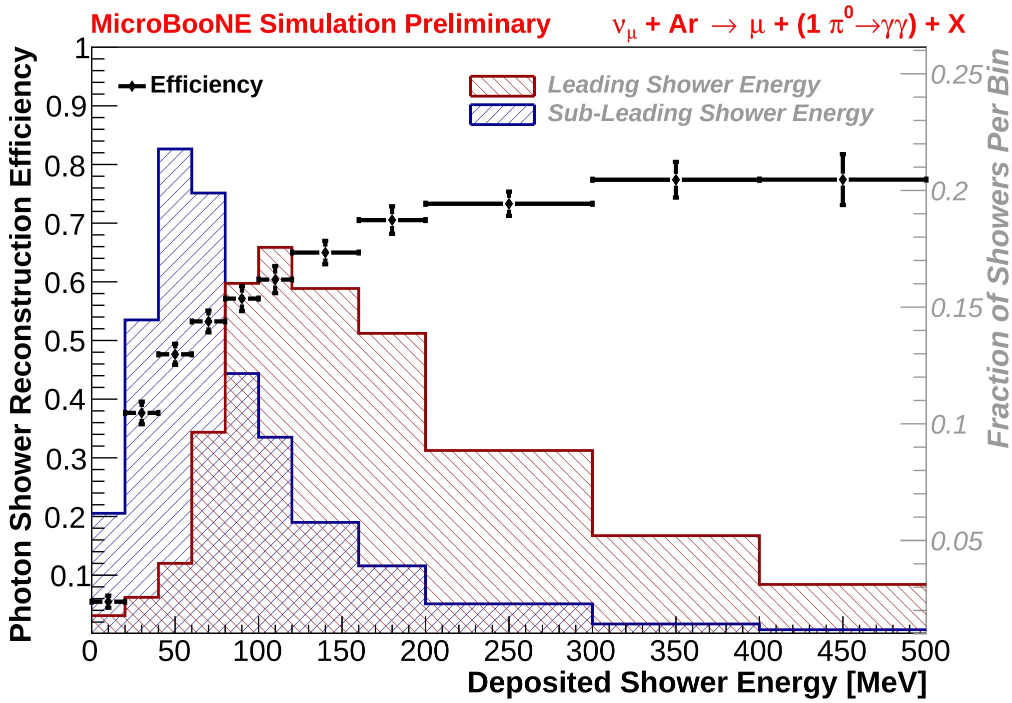

FIG. 1: The $\nu_\mu +\ Ar \to \mu + (1\ \pi^0 \to \gamma\gamma) + X$ shower reconstruction efficiency as a function of the deposited energy of the shower. Overlaid is the energy distribution of the decay photons from neutrino induced π^0 in our simulation. The leading shower in red and the subleading shower in blue.

all of the charge from this particle [22]. These clusters are compared to the neutrino vertex and if they are not well aligned with it they are rejected. Further, if the cluster appears to be too linear or possibly originating from a track-like particle it is rejected [23]. This procedure will struggle for lower energy EM particles, near the Michel spectrum of around 50 MeV, as these will shower in a more stochastic fashion [24] and appear track-like in our readout. In the second stage of EM shower reconstruction the hits designated as shower-like are passed to a re-clustering procedure that works radially from the candidate neutrino vertex using OpenCV, an open source image processing tool [25 and 26]. During image processing all contiguous hits are formed into a 2D cluster on a given plane.

The resulting OpenCV clusters are matched via the time extent of the cluster between the collection plane and one of the two induction planes. With matched clusters, shower properties such as 3D direction and energy from the summed hit charge on the collection plane can be calculated. This shower reconstruction procedure aims to reconstruct photons emanating from neutral pion decays with a clearly defined vertex location.

The algorithm results in highly charge pure showers (on average 92% of the charge comes from the same particle) at the expense of charge completeness (on average 63% of a particles' total charge is collected) which impacts the overall energy resolution. The shower reconstruction efficiency for photons coming from $\nu_\mu + \text{ Ar} \rightarrow \mu + 1\ \pi^0 + X$ interactions as a function of true deposited photon energy is shown in Fig. 1, along with the leading and subleading photon deposited energy distributions. At lower energies we suffer a lower efficiency due to the aggressive targeting of the removal of track-like particles to mitigate cosmic contamination. At these low energies, photons shower appear more track-like. Future improvements can target distinguishing cosmic tracks and low energy photon showers more effectively when projected onto a single plane.

V. Charged Current ν_μ Single π^0 Sample

GENIE predicts that at the neutrino energies of the BNB, if a $\geq$ 50 MeV photon is produced by a neutrino interaction it has a greater than 95% chance of originating from a π^0 decay. To increase our statistics for our cross section we extract results requiring only a single photon, but we will cross check against a sample where both photons are fully reconstructed.

To select this sample from preselected events we require that at least one reconstructed shower point back towards our interaction vertex, with a distance of closest approach of the backward shower projection, or impact parameter, of less than 4 cm, and a start point located within 62 cm of the vertex. These requirements remove showers that are unassociated with the candidate neutrino interaction vertex and result in 771 selected events.

The combined efficiency for selecting ν_μ charged current induced single π^0 events after our preselection, single shower reconstruction efficiency, and above selection is 16% with a purity of 56%. The dominant source of background, 15% of the sample, comes from real EM showers produced near the vertex such as muon radiation and Michel decays, nucleon inelastic scatters, and non-signal π^0 production. A further 8% of the events have a misreconstructed shower selected. Finally, there are two classes of cosmic backgrounds: those selected in a readout window also containing a neutrino interaction and those selected in a readout window containing no neutrino interaction. Together these cosmic backgrounds make up 12% of the sample. The remaining backgrounds come from ν_μ charged current induced single π^0 events outside the fiducial volume (2%), multi-pion events (5%), and neutral current and non-ν_μ charged current interactions (3%). The same degree of agreement between data and simulation, observed at preselection, is observed after this selection. A mis-modeling of uncorrelated activity would appear as an excess of data at large distances, which is not observed.

We fit the 3D distance from the vertex to the reconstructed shower start point to obtain the conversion length. Figure 2 shows the breakdown of the sample into photons created by a neutrino interaction near the vertex, candidate showers correlated with the candidate vertex, candidate showers uncorrelated with the candidate vertex, and purely cosmic backgrounds, where the simulation has

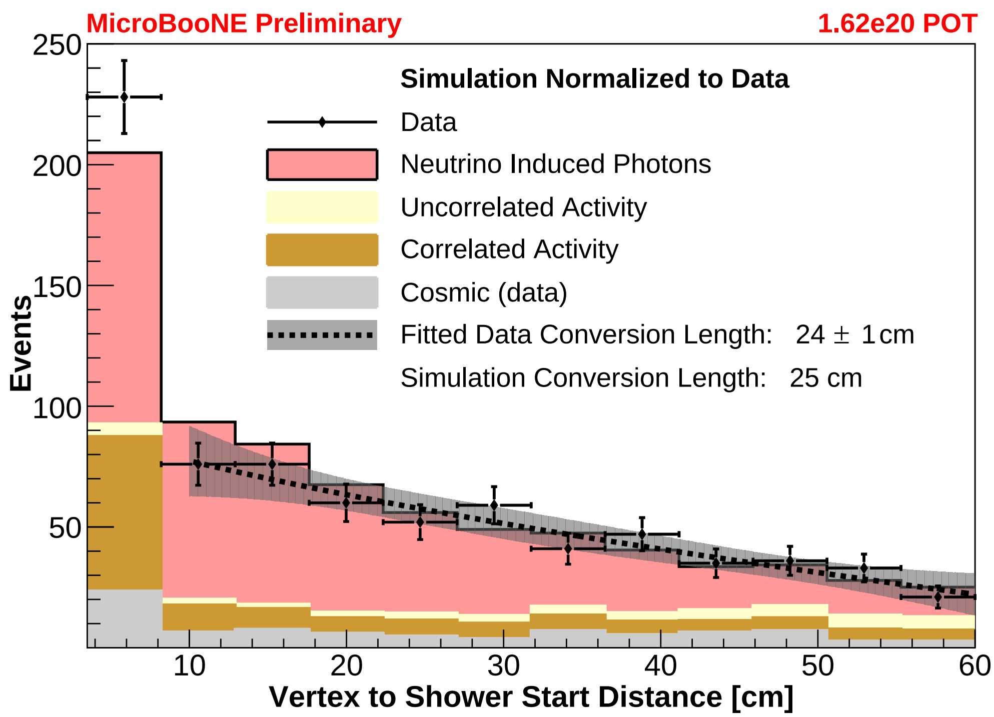

FIG. 2: The vertex to shower start point distance in events we selected as having at least one shower correlated with the neutrino interaction vertex. We separate our simulation into four classes: neutrino-induced photons (red), activity correlated with the candidate vertex (orange), activity uncorrelated with the candidate vertex (yellow), and pure cosmic backgrounds (gray). The simulated neutrino interactions have been area normalized to the data to enable a shape comparison. The fit for these backgrounds and the extracted conversion length excludes the first bin and the uncertainty is purely statistical.

been area normalized to the cosmic-subtracted data. The first bin contains all the showers that are reconstructed from track-like particles, these are correlated to the neutrino interaction and tend to be close to the vertex. To not be biased by these backgrounds we will neglect this first bin and fit the remaining distribution with an exponential plus a linear function. The exponential models the signal and the latter was chosen based on the shape of the simulated backgrounds. The resulting conversion distance of 24 ± 1 (stat.) cm is consistent with our simulation.

VI. π^0 Cross Check Selection

To cross-check this selection we can create a second, further signal enriched, selection by requiring there be at least two showers reconstructed that have a distance of closest approach of their backward shower projections of less than 4 cm. We then sort these two showers into the leading and subleading showers and rely on physical properties of the π^0 decay to help mitigate backgrounds. The leading shower of a π^0 decay cannot have less energy than $m_{\pi^0}/2$, therefore, we require that we have reconstructed at

TABLE I: Comparison of single and two shower selections. There is a significant amount of overlap between the two selections that enables cross checks between selections but lead to large correlations in an extracted cross section measurement.

Selection	ϵ [%]	Selected data events	Overlap[%]	Cosmic backgrounds	Simulated backgrounds
Single Shower	16	771	25.4	86.9	347.3
Two Shower	6	224	87.5	15.3	86.8

least 40 MeV of that energy. At our neutrino energies, showers that are separated by less than 20° are largely the result of a single shower being broken during reconstruction. We reject these events to provide a sample of well-reconstructed events. Finally, we require that the leading and subleading showers convert within 80 cm and 100 cm of the interaction vertex, respectively. If an event has more than one set of candidate showers it is rejected as a background. This two-shower selection increases our sample purity to 64% but with a signal efficiency of only 6%. A direct comparison of the one and two shower selections can be found in Table I. This poor efficiency is driven by that of the subleading photon shower (shown in Fig. 1).

With the two showers we can reconstruct the diphoton mass and check consistency with the π^0 mass. Given that our measured shower energy will be biased downward during the hit removal stage we apply a simulation-based shower energy correction. The two main sources of energy loss in our shower reconstruction occur during hit formation, where some energy will be below the hit finding threshold, and clustering [23]. We apply corrections on the cluster level for each shower to account for these two effects. The diphoton mass distribution is made after these corrections are applied and does not influence these corrections. We find our corrected diphoton mass distribution is consistent with m_{π^0} (Fig. 3). This gives us further confidence that we have selected photons originating from π^0 decays.

VII. Flux-Integrated Total Cross Section

Using our higher efficiency, one shower selection we can proceed to measure a total flux integrated cross section via

$$\left\langle \sigma^{\nu_\mu \mathrm{CC}\pi^0} \right\rangle_\Phi = \frac{N - B}{\epsilon T \Phi}. \tag{1}$$

Here, N is the number of events selected in data (771 events), B is the number of expected background events, ϵ is the efficiency of selecting our signal events, T is the number of argon targets within our fiducial volume, and Φ is the integrated flux through our fiducial volume. We use off-beam data to

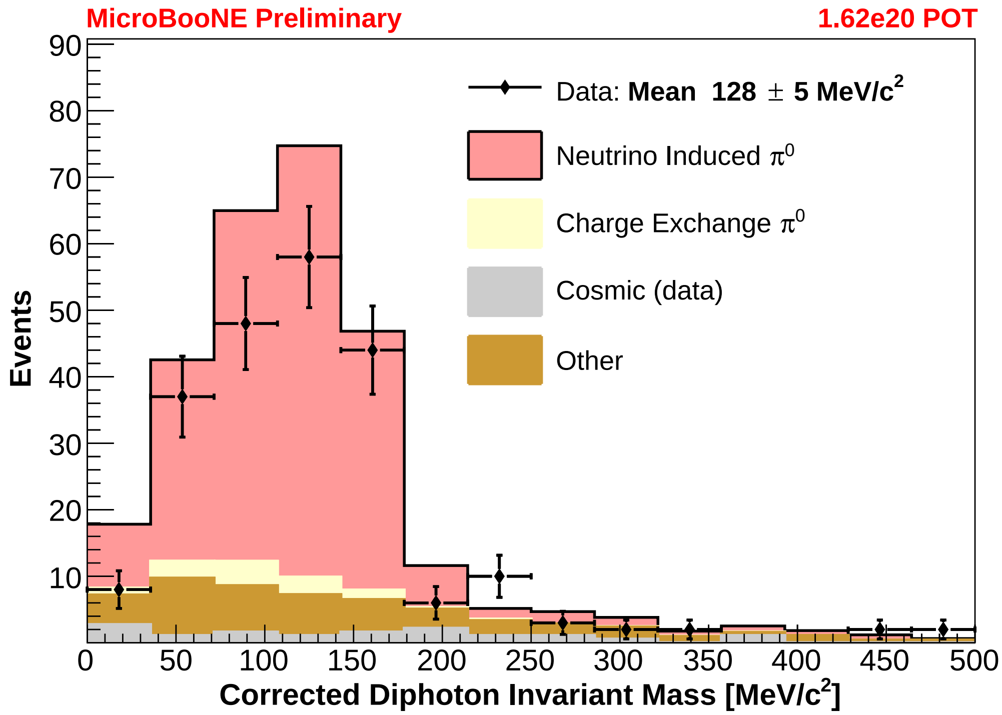

FIG. 3: The reconstructed mass of the two photon candidates associated to the neutrino interaction vertex after an energy scale correction. We separate our simulation into four classes of photon pairs: neutrino-induced π^0 that are created in and subsequently exit the argon nucleus (red), charged pion charge exchange induced $\pi^0 \to \gamma\gamma$ that occur outside the incident argon nucleus (yellow), pure cosmic activity (grey), and everything else (orange). The mean of the data is consistent, within statistical uncertainties, with $m_{\pi^0} = 135$ MeV/c^2.

model the pure cosmic backgrounds (87 events) in B, the remainder (347 events) are taken from the simulation. The impurities in our argon have been measured to be less than 1 ppm, therefore we treat the inner volume as purely argon at 89 K to calculate T. For Φ we integrate the flux from 0 GeV to 3 GeV, shown in Fig. 4. This results in a cross section measurement of

$$\left\langle \sigma^{\nu_\mu \mathrm{CC}\pi^0} \right\rangle_\Phi = (1.94 \pm 0.16 \text{ [stat.]}) \times 10^{-38} \, \frac{\mathrm{cm}^2}{\mathrm{Ar}}. \quad (2)$$

Using our two shower selection we measure a consistent, but highly statistically correlated, cross section.

VIII. Systematic Uncertainties

We address three major sources of uncertainty in this measurement: the interaction models, the neutrino flux prediction, and the detector simulation. Our uncertainties predominantly impact our background estimates, which are solely based on the simulation. Using the default set of GENIE neutrino interaction uncertainties [27] we probe how each modifies our signal efficiency and the simulated neutrino induced

TABLE II: Summary of GENIE systematics uncertainties applied to our cross section measurement through the standard GENIE reweighting framework. We assess the default set of GENIE uncertainties and take the maximum uncertainty for each two-sided variation.

Variation	1σ Uncertainty
Cross Section Parameterization	11.5%
Final State Interactions	10.2%
Hadronization	1.4%
Deep Inelastic Scattering	0.0%
Total Uncertainty	17.2%

TABLE III: Summary of flux systematics uncertainties applied to our cross section measurement using an implementation of the MiniBooNE beamline systematic uncertainty framework ported into LArSoft.

Variation	1σ Uncertainty
p+Be$\rightarrow \pi^+$	11.5%
Beamline	10.2%
p+Be$\rightarrow K^+$	1.4%
p+Be$\rightarrow K^-$	0.4%
p+Be$\rightarrow K^0$	0.4%
p+Be$\rightarrow \pi^-$	0.3%
Total Uncertainty	15.5%

backgrounds. These variations lead to an overall 17% uncertainty on the final extracted cross section. A summary breakdown of the systematics can be found in Table II, while a complete breakdown of each variation is listed in Table V.

To assess the uncertainties on the neutrino flux prediction we utilize the final flux simulation from the MiniBooNE collaboration that have been ported into the LArSoft framework [14]. These account for the hadron production in the beamline, the focusing optics of the secondary pion beam, and the proton counting. As we modify the neutrino flux through our detector we see how the efficiency, simulated backgrounds, and the flux normalization change. Together these lead to a 16% systematic uncertainty on our final cross section measurement. A summary of how each variation impacts our final cross section can be found in Table III.

Finally, to assess uncertainties related to our detector simulation, we vary a wide variety of microphysical effects, such as our electron diffusion model, the scintillation light yield of particles, the electron recombination model [28], and our model of localized electric field distortions. We also vary

TABLE IV: Summary of systematic uncertainties based on detector simulation variations. Each variation is based on a unique set of simulated events. Systematic uncertainty estimates also include contributions from the finite statistics of our simulation.

Variation	1σ Uncertainty
Micro-physics	12.9%
Detector Response	12.5%
Cosmic Simulation	11.0%
Total Uncertainty	21.1%

our simulated detector response to account for uncertainties in the modeling of effects such as the single photon rate observed in our PMTs, the data-driven noise model [19], the data-driven signal response, the channels that tend to become intermittently non-responsive, the visibility of the region surrounding our TPC to our PMT array, and the simulation of long-range induced signals on our wires [20]. We create an independent detector simulation for each of these variations, treated as fully uncorrelated. These independent simulations result in a statistical uncertainty that must be assessed when estimating the systematic uncertainty. We measure the size of the systematic uncertainty by extracting the cross section from each independent simulation, measure the percent difference from a central value simulation, and then add the simulation-based statistical uncertainty in quadrature. For our two shower selection the low efficiency coupled with the finite statistics of these simulations leads us to only be sensitive to systematic effects greater than 6%. We also assess a systematic uncertainty on the reconstructed neutrino interactions that are contaminated by simulated cosmic activity. This is taken as a 100% normalization uncertainty, and leads to a 11% systematic uncertainty on the final cross section measurement. A summary of these systematic uncertainties can be found in Table IV.

The combined uncertainty on our measurement is 31% and we obtain,

$$\left\langle \sigma^{\nu_\mu \mathbf{CC}\pi^0} \right\rangle_\Phi = (1.94 \pm 0.16 \text{ [stat.]} \pm 0.60 \text{ [syst.]}) \times 10^{-38} \, \frac{\text{cm}^2}{\text{Ar}}. \tag{3}$$

We compare this measurement with two sets of models implemented in GENIE. The first is the default with an empirical MEC model and utilizes a Bodek-Ritchie Fermi Gas model [29 and 30] for the initial nucleon energy distribution and a Rein-Sehgal model [31] for the resonant production. The second model set uses a Local Fermi Gas model for the initial nucleon energy distribution, a Berger-Sehgal model [32] for the resonant production, and has an updated tuning of the hadron transport model. These are compared to our measured cross section in Fig. 4. We find that our data is consistent, within 1.2σ, with the default GENIE model.

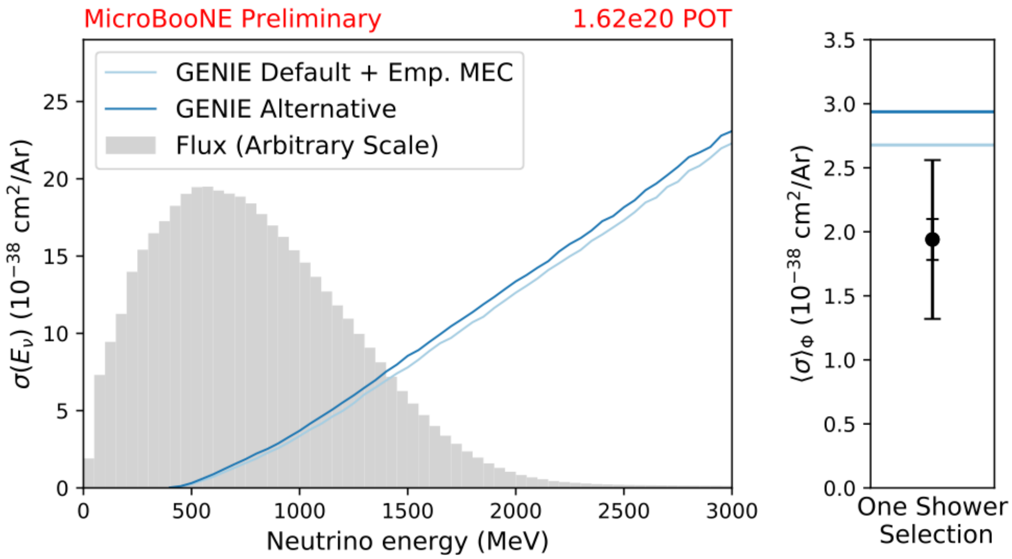

FIG. 4: The measured total flux integrated ν_μ charged current single pion cross section, right panel, with the inner error bars denoting the statistical uncertainty and the outer error bars denote the quadratic sum of statistical and systematic uncertainties. The left panel shows the full BNB flux (gray) we integrate over and the two GENIE cross sections we compare our measurement to.

IX. Conclusions

In conclusion, MicroBooNE has utilized the first implementation of a fully automated electromagnetic shower reconstruction to measure the first charged current neutral pion cross section on argon. This measurement is in agreement with the default GENIE plus empirical MEC prediction for this process. The dominant systematic uncertainty in this analysis arises from the detector modeling. Future improvements in our sense wire signal modeling and signal extraction procedure should aid in mitigating the impact of these effects [20 and 21]. Furthermore, future analyses can improve on the shower reconstruction by utilizing a better track-shower separation as an input to the clustering stage. This would enable us to explore kinematic properties on the π^0 decay and provide a more robust constraint of the backgrounds to mitigate the model dependence. Together these will enable us to extract a differential cross section as a function of the π^0 kinematics to test models of final state interactions and nuclear effects.

X. Acknowledgements

We acknowledge the support of the Fermi National Accelerator Laboratory (Fermilab). Fermilab is managed by Fermi Research Alliance, LLC (FRA), acting under Contract No. DE-AC02-07CH11359.

MicroBooNE is supported by the following: the U.S. Department of Energy, Office of Science, Offices of High Energy Physics and Nuclear Physics; the U.S. National Science Foundation; the Swiss National Science Foundation; the Science and Technology Facilities Council of the United Kingdom; and The Royal Society (United Kingdom). Additional support for the laser calibration system and cosmic ray tagger was provided by the Albert Einstein Center for Fundamental Physics, Bern, Switzerland.

A. Appendix: Auxiliary Plots

These plots act to supplement the above analysis. These include the candidate muon track length at preselection and after the single shower selection, shown if Fig. 5. These include the GENIE and neutrino flux uncertainties to help convey the size of our normalization uncertainties. In Fig. 6 we have the number of showers reconstructed in the events before and after the single shower selection.

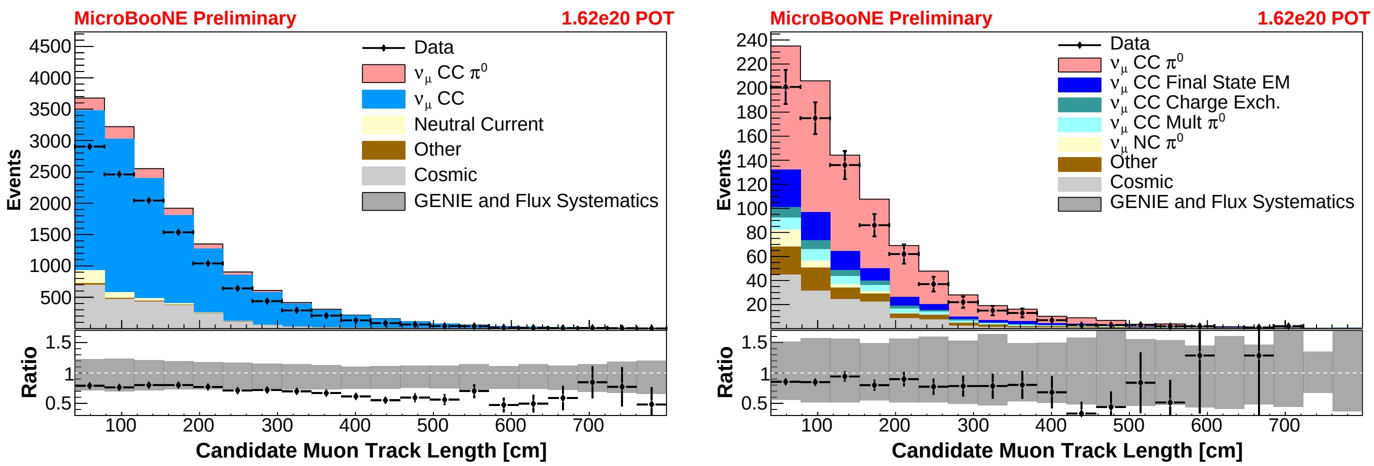

FIG. 5: The distribution of candidate muon track lengths after preselection (left) and after the one shower selection (right). The data points represent the statistical uncertainties and the band on the ratio correspond to the GENIE and neutrino flux uncertainties.

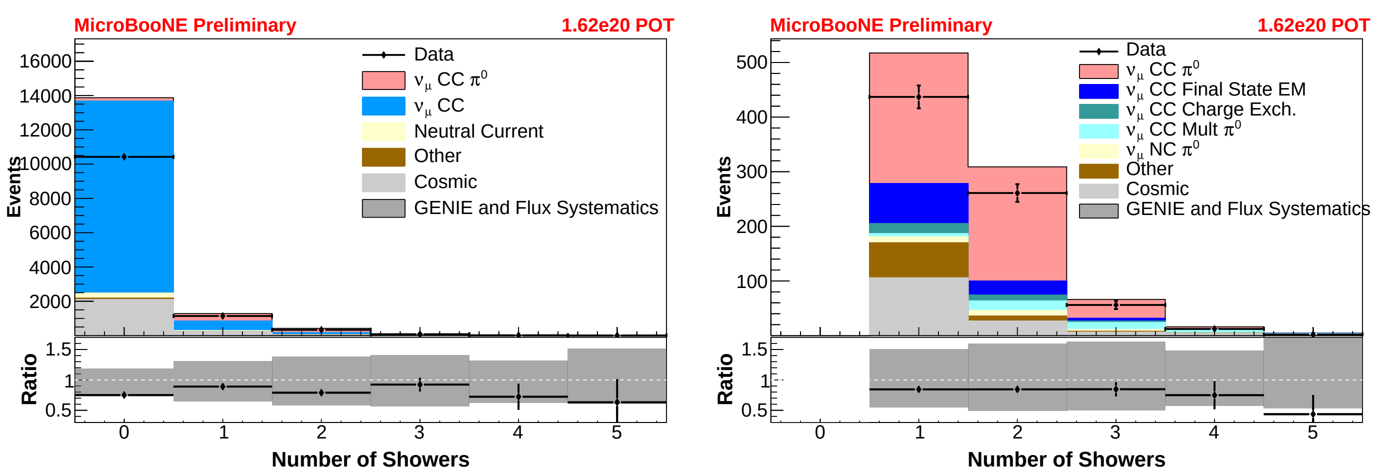

FIG. 6: The number of reconstructed showers after preselection (left) and after the one shower selection (right). The data points represent the statistical uncertainties and the band on the ratio correspond to the GENIE and neutrino flux uncertainties.

B. Appendix: Diphoton Invariant Mass Comparison

We can gauge the extent to which our shower reconstruction is performing by comparing it directly to energy resolution required in the DUNE CDR and SBN Program Proposal. To do this we can subtract all physics backgrounds from our diphoton invariant mass and plot our area normalized signal simulation. We can then take the true deposited energy of the events that are selected by our selection and then randomly sample from a Gaussian with a mean at the deposited energy of that shower and a width quoted in the proposals. The opening angle between the two showers is also smeared based on the angular resolution listed in the proposals. The angular resolution contributes largely to the higher mass tail. Each event is sampled many times and a diphoton invariant mass is created. This distribution of events would be the shape of the diphoton invariant mass if our shower reconstruction had the energy resolution listed in these proposals, shown in Fig. 7. We find that our reconstructed mass distribution is 20% more narrow than the DUNE and SBN Program Proposal distributions based on the full-width half-maxima.

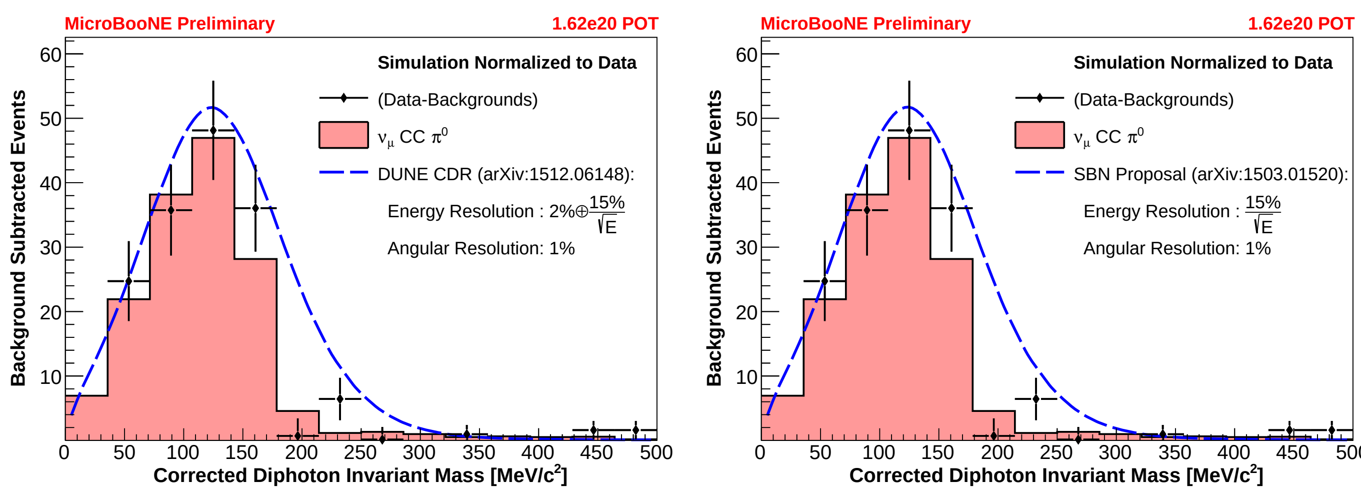

FIG. 7: Comparison of our background subtracted diphoton invariant mass distribution (black) to our area normalized simulated signal events ($\nu_\mu + Ar \rightarrow \mu + 1\pi^0 + X$) (salmon histogram). This compared to the diphoton mass distribution that would be achieved with an energy and angular resolution listed in the DUNE CDR (left) and the SBN Program Proposal (right).

C. Appendix: Diphoton Invariant Mass Input Plots

When calculating the diphoton invariant mass for our two shower selection it is also interesting to look at the distributions that go into its calculation. These three quantities are the corrected leading shower energy (shown in Fig. 8), the corrected subleading shower energy (shown in Fig. 9), and the two shower

3D opening angle (shown in Fig. 10). The simulation is presented both POT normalized (to the left in all figures) and area normalized to the data (to the right in all the figures).

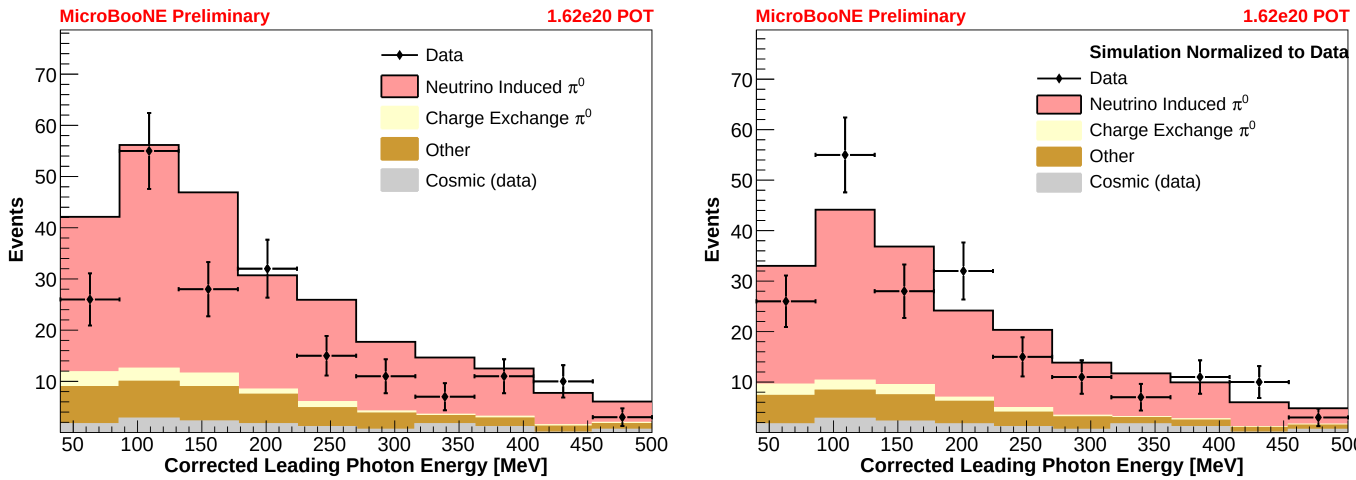

FIG. 8: The distribution of the corrected leading shower energy with the simulation POT normalized (left) and area normalized to the data (right).

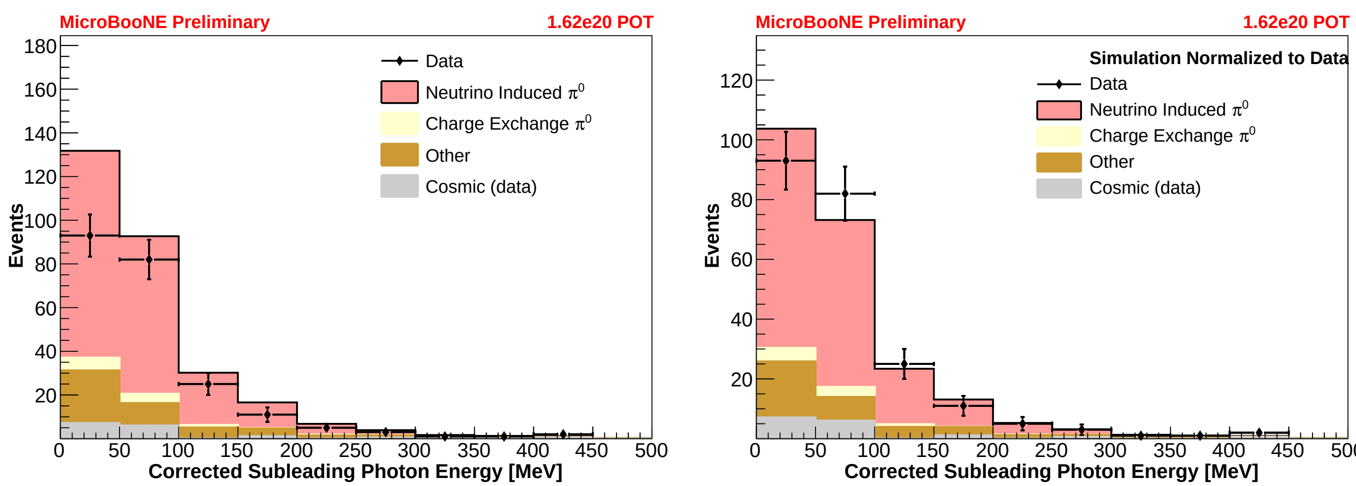

FIG. 9: The distribution of the corrected subleading shower energy with the simulation POT normalized (left) and area normalized to the data (right).

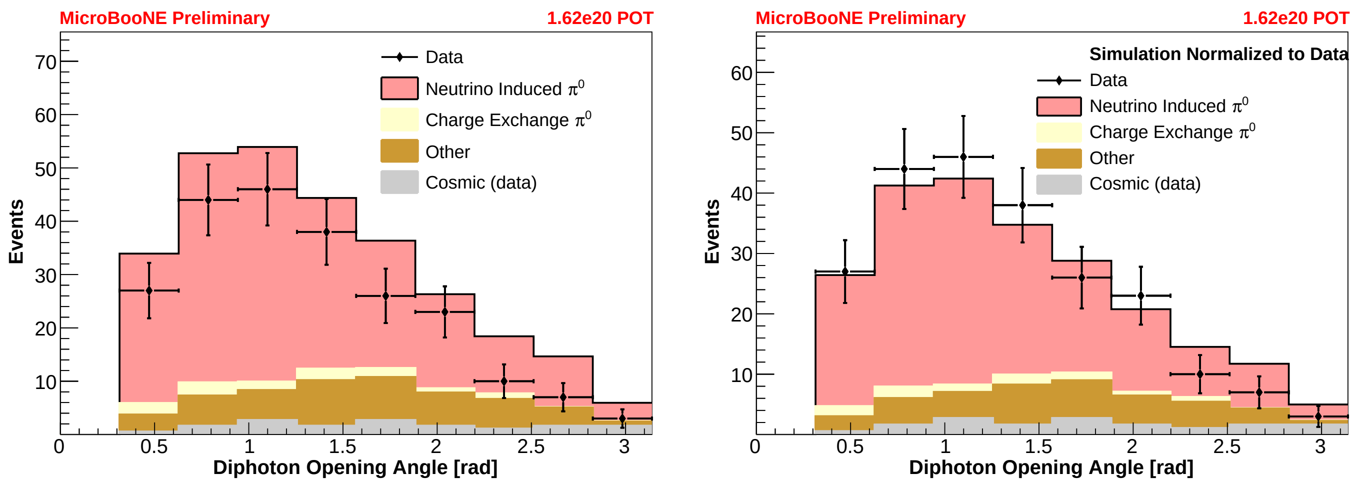

FIG. 10: The distribution of the two shower 3D opening angle with the simulation POT normalized (left) and area normalized to the data (right).

D. Appendix: Full Cross Section Uncertainty Table

Table V lists each variation available within the GENIE reweighting framework and how it shift our measured cross section.

References

[1] C. Rubbia, CERN-EP-INT-77-08 (1977).

[2] R. Acciarri *et al.* (ArgoNeuT), Phys. Rev. **D95**, 072005 (2017).

[3] R. Acciarri *et al.* (DUNE), (2015), arXiv:1512.06148 [physics.ins-det].

[4] M. Antonello *et al.* (LAr1-ND, ICARUS-WA104, MicroBooNE), (2015), arXiv:1503.01520 [physics.ins-det].

[5] R. Acciarri *et al.* (MicroBooNE), JINST **12**, P02017 (2017), arXiv:1612.05824 [physics.ins-det].

[6] A. A. Aguilar-Arevalo *et al.* (MiniBooNE), Phys. Rev. Lett. **110**, 161801 (2013), arXiv:1303.2588 [hep-ex].

[7] S. J. Barish *et al.*, Phys. Rev. D **19**, 2521 (1979).

[8] G. M. Radecky *et al.*, Phys. Rev. D **25**, 1161 (1982).

[9] T. Kitagaki *et al.*, Phys. Rev. D **34**, 2554 (1986).

[10] T. Le *et al.*, Physics Letters B **749**, 130 (2015).

[11] O. Altinok *et al.* (MINERvA), Phys. Rev. **D96**, 072003 (2017), arXiv:1708.03723 [hep-ex].

[12] J. Catala-Perez, *Measurement of neutrino induced charged current neutral pion production cross section at SciBooNE.*, Ph.D. thesis, Valencia U., IFIC (2014).

[13] A. A. Aguilar-Arevalo *et al.* (MiniBooNE Collaboration), Phys. Rev. D **83**, 052009 (2011).

[14] A. A. Aguilar-Arevalo *et al.* (MiniBooNE), Phys. Rev. **D79**, 072002 (2009), arXiv:0806.1449 [hep-ex].

[15] C. Andreopoulos *et al.*, Nucl. Instrum. Meth. **A614**, 87 (2010), version 2.12.00, arXiv:0905.2517 [hep-ph].

[16] T. Katori, *Proceedings, 8th International Workshop on Neutrino-Nucleus Interactions in the Few GeV Region (NuInt 12): Rio de Janeiro, Brazil, October 22-27, 2012*, AIP Conf. Proc. **1663**, 030001 (2015), arXiv:1304.6014 [nucl-th].

[17] E. D. Church, (2013), version v06.26.01.12, arXiv:1311.6774 [physics.ins-det].

[18] D. Heck, G. Schatz, T. Thouw, J. Knapp, and J. N. Capdevielle, (1998), version v7.4003 with constant mass composition model.

[19] R. Acciarri *et al.* (MicroBooNE), JINST **12**, P08003 (2017), arXiv:1705.07341 [physics.ins-det].

TABLE V: Results from GENIE event reweighting on our extracted cross section.

Variation	1σ Uncertainty
M_A^{NCEL}	0.3%
η^{NCEL}	0.0%
M_A^{CCQE}	3.4%
M_V^{CCQE}	0.2%
M_A^{CCRES}	10.1%
M_V^{CCRES}	5.9%
M_A^{NCRES}	1.7%
M_V^{NCRES}	0.5%
$M_A^{COH}\pi$	0.3%
$R_0^{COH}\pi$	0.3%
AGKYpT	0.0%
AGKYxF	0.0%
DISAth	0.2%
DISBth	0.3%
DISCν1u	0.2%
DISCν2u	0.2%
FormZone	3.6%
BR (γ)	0.2%
BR (η)	2.7%
BR (θ)	2.7%
$RR_{\nu p}^{CC1\pi}$	1.1%
$RR_{\nu p}^{CC2\pi}$	2.6%
$RR_{\nu n}^{CC1\pi}$	4.1%
$RR_{\nu n}^{CC2\pi}$	2.2%
x_{abs}^N	1.9%
x_{cex}^N	0.8%
x_{el}^N	3.3%
x_{inel}^N	0.5%
x_{mfp}^N	4.0%
x_{π}^N	0.5%
x_{abs}^{π}	5.1%
x_{cex}^{π}	0.1%
x_{el}^{π}	0.5%
x_{inel}^{π}	5.4%
x_{mfp}^{π}	0.7%
x_{π}^{π}	0.4%
Total Uncertainty	17.2%

[20] C. Adams *et al.* (MicroBooNE), (2018), arXiv:1802.08709 [physics.ins-det].

[21] C. Adams *et al.* (MicroBooNE), (2018), arXiv:1804.02583 [physics.ins-det].

[22] R. Acciarri *et al.* (MicroBooNE), Eur. Phys. J. **C78**, 82 (2018), arXiv:1708.03135 [hep-ex].

[23] D. Caratelli, *Study of Electromagnetic Interactions in the MicroBooNE Liquid Argon Time Projection Chamber*, Ph.D. thesis, Columbia U. (2018).

[24] R. Acciarri *et al.* (MicroBooNE), JINST **12**, P09014 (2017), arXiv:1704.02927 [physics.ins-det].

[25] G. Bradski, Dr. Dobb's Journal of Software Tools (2000).

[26] A. Hackenburg, *Measurement of a Neutrino-Induced Charged Current Single Neutral Pion Cross Section at MicroBooNE*, Ph.D. thesis, Yale U. (2018).

[27] C. Andreopoulos, C. Barry, S. Dytman, H. Gallagher, T. Golan, R. Hatcher, G. Perdue, and J. Yarba, (2015), arXiv:1510.05494 [hep-ph].

[28] R. Acciarri *et al.* (ArgoNeuT), JINST **8**, P08005 (2013), arXiv:1306.1712 [physics.ins-det].

[29] A. Bodek and J. L. Ritchie, Phys. Rev. D **23**, 1070 (1981).

[30] A. Bodek and J. L. Ritchie, Phys. Rev. D **24**, 1400 (1981).

[31] D. Rein and L. M. Sehgal, Annals of Physics **133**, 79 (1981).

[32] C. Berger and L. M. Sehgal, Phys. Rev. **D79**, 053003 (2009), arXiv:0812.2653 [hep-ph].